

Results of search for magnetized quark-nugget dark matter from radial impacts on Earth

J. Pace VanDevender^{1*}, Robert G. Schmitt², Niall McGinley³, David G. Duggan⁴,
Seamus McGinty⁵, Aaron P. VanDevender¹, Peter Wilson⁶, Deborah Dixon⁷, Helen Girard¹,
and Jacquelyn McRae¹

- 1 VanDevender Enterprises LLC, 7604 Lamplighter Lane NE, Albuquerque, NM 87109 USA; pace@vandevender.com
- 2 Sandia National Laboratories, Albuquerque, NM 87185-0840, USA; pace@vandevender.com
- 3 Ardaturr, Churchill PO, Letterkenny, Co. Donegal, Ireland; niallmacfhionghaile@gmail.com
- 4 National Park and Wildlife Service, Glenveagh National Park, Church Hill, County Donegal, F92XK02, Ireland; dave.duggan@chg.gov.ie
- 5 Church Hill, Letterkenny, County Donegal, F928982, Ireland, pace@vandevender.com
- 6 School of Geography and Environmental Sciences, Ulster University, Cromore Road, Coleraine, Co. Londonderry, BT52 1SA Northern Ireland, UK; p.wilson@ulster.ac.uk
- 7 DKD Engineering Inc., 801 El Alhambra Cir. NW, Los Ranchos, NM 87107, USA; ddixon@dkdengineeringinc.com

*Correspondence: pace@vandevender.com

Abstract: Magnetized quark nuggets (MQNs) are a recently proposed dark-matter candidate consistent with the Standard Model and with Tatsumi's theory of quark-nugget cores in magnetars. Previous publications have covered their formation in the early universe, aggregation into a broad mass distribution before they can decay by the weak force, interaction with normal matter through their magnetopause, and first observation consistent MQNs: a nearly tangential impact limiting their surface-magnetic-field parameter B_0 from Tatsumi's $\sim 10^{12+/-1}$ T to 1.65×10^{12} T +/- 21%. The MQN mass distribution and interaction cross section depend strongly on B_0 . Their magnetopause is much larger than their geometric dimensions and can cause sufficient energy deposition to form non-meteorite craters, which are reported approximately annually. We report computer simulations of the MQN energy deposition in water-saturated peat, soft sediments, and granite and report results from excavating such a crater. Five points of agreement between observations and hydrodynamic simulations of an MQN impact support this second observation consistent with MQN dark matter and suggest a method for qualifying additional MQN events. The results also redundantly constrain B_0 to $\geq 4 \times 10^{11}$ T. MQN events. The results also redundantly constrain B_0 to $\geq 4 \times 10^{11}$ T.

Keywords: dark matter; quark nugget; magnetized quark nugget; MQN; nuclearite; magnetar; strangelet; slet; Macro

1. Introduction

Dark matter [1-6] comprises about 85% of the mass in the universe. After decades of searches for experimental and observational evidence supporting any of many candidates for

dark matter, the nature of dark matter is still a mystery [6-7]. A quark nugget is a dark-matter candidate composed of up, down, and strange quarks [8-15]. Quarks are constituents of many particles in the Standard Model of Particle Physics [16]. Quark nuggets are a Standard-Model candidate for dark matter that has not been excluded by observations [13,15]. A current summary of quark-nugget research can be found in reference [17].

Most models of quark nuggets do not include effects of their intrinsic magnetic field. However, Xu [18] has shown that the low electron density, permitted in stable quark nuggets, limit surface magnetic fields from ordinary electron ferromagnetism to $\sim 2 \times 10^7$ T. Tatsumi [19] examined ferromagnetism from a One Gluon Exchange interaction and concluded that the surface magnetic field could be sufficient to explain the $\sim 10^{12+/-1}$ T magnetic fields inferred for magnetar cores. Since the result depends on the currently unknown value of α_c at the 90 MeV energy scale, the result needs to be confirmed with relevant observations and/or advances in QCD calculations.

Since magnetars exist [20] with magnetic field ~ 300 times that of neutron-star pulsars [21] and since such a large magnetic field is uniquely consistent with ferromagnetic quark nuggets, we are exploring the implications of such Magnetized Quark Nuggets (MQNs) as candidates for dark matter. Previously published theoretical results [15] show their origin was at time $t \sim 65 \mu\text{s}$ when the Universe had a temperature of ~ 100 MeV according to the Standard Model of Cosmology [2]. At that temperature, Λ^0 particles (consisting of one up, one down, and one strange quark) could form [22] and magnetically aggregate [15] into a broad mass distribution of stable ferromagnetic MQNs before they could decay. In the extremely high mass density of the early Universe, aggregation happened faster than the ~ 10 ps decay by the weak interaction. Since current day accelerator experiments have a much lower mass density, aggregation does not compete with decay, so stable MQNs are not formed in those experiments.

After $t \approx 66 \mu\text{s}$ after the big bang, mean MQN mass is between $\sim 10^{-6}$ kg and $\sim 10^4$ kg, depending on the surface magnetic field B_0 . The corresponding mass distribution is sufficient for MQNs to meet the requirements [13,15] of dark matter in the subsequent processes, including those that determine the Large Scale Structure (LSS) of the Universe and the Cosmic Microwave Background (CMB).

Throughout this paper, we will use B_0 as a key parameter that defines the mass distribution of MQNs. The value of B_0 equals Tatsumi's surface magnetic field B_s if the mass density of MQNs $\rho_{QN} = 10^{18}$ kg/m³ and the density of dark matter was $\rho_{DM} = 1.6 \times 10^8$ kg/m³ when the temperature of the universe was ~ 100 MeV [15,22]. If better values of ρ_{QN} and ρ_{DM} are found, then the corresponding values of B_s can be calculated by multiplying the B_0 from our results by $(1 \times 10^{-18} \rho_{QN}) (6.25 \times 10^{-9} \rho_{DM})$.

MQNs interact with surrounding matter [23] through the magnetopause effect, which provides at least three measurable signatures of MQN dark matter:

1) hypervelocity (> 3 km/s) atmospheric transit without luminous streak and without breakup in an air shower [24] but with energetic (> 1 kJ/m) energy deposition and with multi-meter transit through solid-density matter,

2) electromagnetic emissions (kHz to GHz) from the rotating magnetic dipole after transit through matter [25], and

3) magnetic levitation of rotating MQN magnetic dipole after transit through matter [17] by induced currents in adjacent conducting material or magnetic levitation of static magnetic dipole above a superconductor.

A systematic attempt to detect MQNs through the first signature was attempted [23] by looking for acoustic signals from MQN impacts in the Great Salt Lake in Utah, USA. Even though the first method monitored ~ 30 sq-km (i.e. ~ 30 times the cross section of the IceCube Neutrino Observatory at the South Pole) for impacts with MQN mass $\geq 10^4$ kg, none were detected [15]. The null results implied that analysis based on average mass, which is the usual assumption for dark-matter candidates, may be inadequate and motivated the detailed computation of the MQN mass distribution. Those results show a much larger detector and/or much longer observation times are required.

Reference [25] describes how MQNs passing through matter spin up to MHz frequencies and emit radiofrequency energy (the basis of the second signature) and proposes using Earth's magnetosphere as a sufficiently large detector to get enough events. The large uncertainty in B_0 from Tatsumi's theory is a major impediment to designing and fielding such an experiment.

Reference [17] describes an extremely rare episodic observation and supporting simulations of the third method. That method is too rare to provide enough data to measure the mass distribution and provide sufficient statistics for discovery of MQNs. However, those results do limit the key parameter B_0 to $1.3 \times 10^{12} \text{ T} \leq B_0 \leq 2 \times 10^{12} \text{ T}$ and permit the design of the systematic experiment based on the second signature with Earth's magnetosphere as the detector area.

Such a project requires major investment. Additional episodic data would help justify the project. The current paper provides additional episodic observational and supporting computational results of the first method, based on non-meteorite crater impacts on Earth. We also discuss extending the results to find a statistically significant number of MQN impacts.

We use the terms meteors and meteorites to refer to bodies composed of normal matter, i.e. atoms held together by the electromagnetic force. The material strength associated with the electromagnetic force is weak. Thus, meteors and meteorites (as defined in this paper) must be quite large to survive intact and do not make small craters. Nuclear-density quark nuggets are held together by the strong-nuclear force, so all of them survive passage through the atmosphere.

Craters that show no evidence of meteorite impact are reported in the press approximately once per year. Therefore, the event rate for non-meteorite craters is sufficient to allow the phenomenon to be studied, if access to the craters can be obtained. Three events in three years have been recently reported.

1. A 12-m diameter crater was reported near Managua, Nicaragua, on September 6, 2014 [Cooke, W. Did a meteorite cause a crater in Nicaragua? http://blogs.nasa.gov/Watch_the_Skies/2014/09/08/did-a-meteorite-cause-a-crater-in-nicaragua/ and <http://www.cnn.com/2014/09/08/tech/innovation/nicaragua-meteorite/>, (2014) (Date of access: 02/14/2021)].

2. Another event occurred on July 4, 2015, at the Salty Brine Beach in Rhode Island, USA [Shapiro, E., Cathcart, C. & Donato, C. Bomb squad, ATF investigating mysterious explosion at Rhode Island beach. <http://abcnews.go.com/US/explosion-report-prompts-evacuation-rhode-island-beach/story?id=32384143>, (2015) (Date of access: 02/14/2021)].

3. On February 6, 2016, an event occurred in Tamil Nadu, India [Hauser, C. That wasn't a meteorite that killed a man in India, NASA says. http://www.nytimes.com/2016/02/10/world/asia/that-wasnt-a-meteorite-that-killed-a-man-in-india-nasa-says.html?_r=0, (2016) (Date of access: 02/14/2021)].

None of these impacts was preceded by a luminous track in the sky. No meteorite material was found in or near any of the craters. Impact experts who reviewed the news reports concluded that these events were not meteorite impacts. In the absence of a scientific basis for impacts that form craters without luminous tracks and without meteorite fragments, these experts attributed them to human-caused explosions by default. Our results indicate that MQNs can cause non-meteorite craters, not just human-caused explosions.

Each non-meteorite event provides a large-target opportunity to test the MQN dark-matter hypothesis. Since a multi-layer witness plate provides more information than a single-layer one, peat bogs on top of soft sediments and bedrock offer particularly useful opportunities. Sections 3.1 through 3.2 report results of hydrodynamic simulations and analyses of MQNs interacting with a three-layer witness plate of peat, clay-sand mixture, and granite bedrock in County Donegal, Ireland. Other peat bogs could also provide such opportunities. However, County Donegal has the advantages of 1) a granite bedrock within excavation range of the surface, 2) a friendly and supportive population, 3) a governing authority over peat bogs that can grant permits for exploration, and 4) maximum exposure to the directed flux of dark matter. The last advantage arises because dark matter streams into Earth as the solar system moves around the galactic center and through the dark-matter halo. That direction of motion is right ascension 18h 36m 56.33635s, declination +38° 47' 01.2802" and is always above the horizon for latitudes greater than that declination, including the latitude of County Donegal.

Sections 3.4 through 3.8 report the observations and associated analyses from excavating a non-meteorite impact that occurred in County Donegal in May of 1985. We find the crater and subsurface damage to be consistent with an MQN impact that deposited ~ 80 MJ/m in the water-saturated peat. The corresponding MQN mass depends on the value of B_0 . MQN mass distributions consistent with ~ 80 MJ/m energy deposition provide an additional exclusion of $B_0 < 4 \times 10^{11}$ T. For the most likely range of $1.3 \times 10^{12} \text{ T} \leq B_0 \leq 2 \times 10^{12} \text{ T}$, ~ 80 MJ/m energy deposition corresponds to MQN mass of 5 ± 1 kg.

Section 4 discusses the results, alternative explanations, and a potential method for more efficiently determining if a candidate impact is consistent with a deeply penetrating MQN impact or with some surface phenomenon. In principle, such a method could locate additional MQN events.

Editorial policy for this journal requires authors declare if an article is controversial. For the last four decades, searches for dark-matter candidates have focused on particles that are Beyond the Standard Model (BSM) of Particle Physics. Since MQNs are composed of Standard Model quarks and the theory for the ferromagnetic state of MQNs is an approximate solution within the Standard Model, the MQN hypothesis for dark matter does not require a BSM particle and may be considered controversial by the BSM community. However, a potential solution to dark matter for the Standard Model of Cosmology and not requiring a hypothetical BSM particle may be less controversial to others because it is a modest extension of well-established physics.

We report the results from just one episodic event, which we calculate in section 4.2 to have a $< 2\%$ of arising randomly from unknown effects. Nevertheless, we conclude that many more instances are required to determine whether or not MQNs exist and contribute to dark matter. The event presented in this paper suggests a method for adding more instances of MQN interaction by qualifying other non-meteorite impacts, which occur approximately annually.

2. Materials and Methods

This study used

1. Computational 2D and 3D hydrodynamic simulations, described in results section and in movies of pressure, mass density, and temperature in supplementary dataset at <https://doi.org/10.5061/dryad.cc2fqz641> and associated analyses of energy deposition in the multi-layers of peat bog in the results section;
2. Original field work at the location of a non-meteorite impact in May of 1985 in County Donegal, Ireland, and associated analyses in the results section;
3. Additional details in Appendix A: Excavations, to assist an independent team to extend our findings; and
4. Potential sites in Appendix B: Coordinates and description of deformations in peat-bog survey, for future investigations if suitable sensor technology can be developed.

3. Results

3.1 Hydrodynamic simulation of MQN impact in three-layer witness plate

Two and three dimensional simulations with the CTH hydrodynamics simulation software [26,27] were conducted to investigate MQN interactions with a three-layer witness plate of peat-bog, clay-sand mixture, and granite bedrock. Two dimensional simulations examined the craters formed by MQN impacts as a function of MQN mass and the B_0 parameter. Three dimensional simulations investigated the circularity of the crater as a function of angle relative to vertical and guided the excavation of an impact site in County Donegal, Ireland.

In both cases, the MQN deposits energy along its path and within the magnetopause [23] radius (e.g. ~ 1 mm radius for a 30 MJ/m energy deposition from a 1-kg MQN for $B_0 \approx 10^{12}$ T). The interaction produces a plasma with initial temperature of $\sim 2,100$ eV. Turbulent mixing with colder material is assumed to dominate the early dynamics of the interaction and produces a channel of larger radius and lower temperature. Hydrodynamic pressure drives radial motion of the channel and venting of plasma to the atmosphere to form the crater.

Therefore, we approximate the hydrodynamic phase of the plasma channel as a cylinder with the mass density of the peat, clay-sand, or granite. Temperature was varied from 0.5 to 1.55 eV and the radius was varied to give the specified energy per unit length. The results were essentially independent of temperature over that range and validated the assumption that energy/length is the dominant variable. For a given material and temperature, the initial radius of the channel was chosen to give the desired energy/length based on the SESAME4 [27] equation of state.

The fluid above the peat was atmosphere at standard temperature and pressure. The simulated depth of the peat was the actual 0.7 m of the Irish peat bog with initial density of 1.12×10^3 kg/m³ and sound speed of 1.46×10^3 m/s. The 4.7 m-thick clay-sand layer was simulated with a 1.0 meter thick layer and with initial density of 2.02×10^3 kg/m³ and sound speed of 2.2×10^3 m/s. The granite layer was simulated with a 0.3-m layer with initial density of 2.6×10^3 kg/m³ and sound speed of 5.0×10^3 m/s. The bottom of each simulation was unmovable, and material could freely exit from the other boundaries.

Two-dimensional hydrodynamic simulations were conducted with 1, 3, 9, 27, 81, and 243 MJ/m energy deposition. They show that a shock wave reflects off the mass discontinuities and propagates radially outward in all three layers. Low-density and high-temperature material in the central channel is ejected into the atmosphere. Lower temperature material behind the shock wave moves radially and almost one-dimensionally outward. Finally, the peat distorts two-dimensionally in response to the velocity field it has acquired and the shear planes that have developed within the peat.

Representative results of the density maps, when material velocities are well below their peak values, are shown in Figure 1.

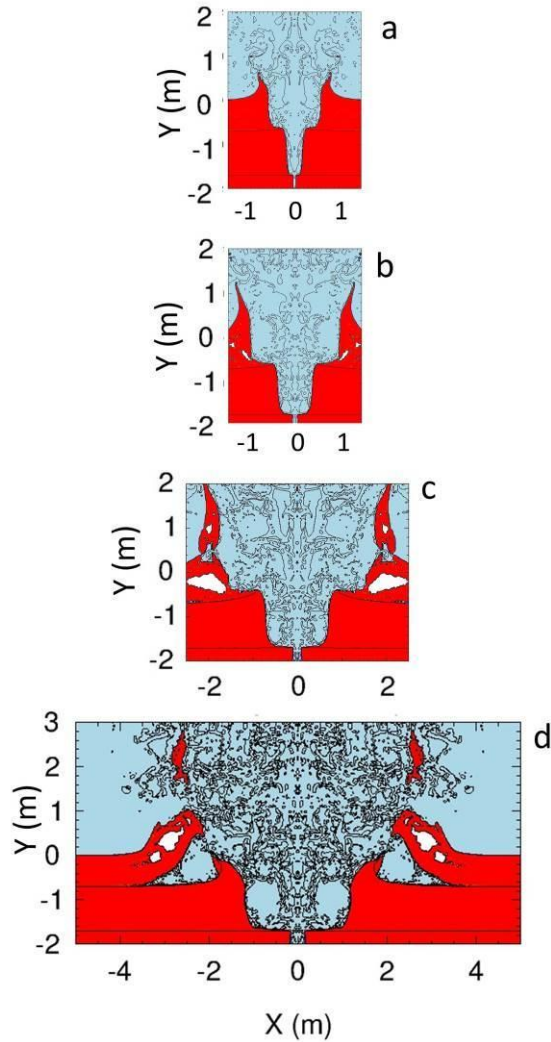


Figure 1. Representative density maps are shown for a) 9 MJ/m, b) 27 MJ/m, c) 81 MJ/m, and d) 243 MJ/m. The red material represents three layers from the bottom up: 0.3 m of granite, 1.0 m of clay-sand, and 0.7 m of peat with initial density of $1.12 \times 10^3 \text{ kg/m}^3$. The blue area is atmospheric air.

The 81 MJ/m case in Figure 1c is especially relevant to the crater discussed below. The shear planes and voids form relatively smooth sides of the peat crater. Most of the peat is ejected in small fragments into the atmosphere. Larger pieces of peat are shown as vertical pieces about to be ejected radially away from the crater. The channel is almost one-dimensional in the clay-sand and in the granite. Movies of the pressure, density, and temperature of the 81 MJ/m case are available at <https://datadryad.org/stash/share/Lt7dMvxEAUWNnkfKt2xPg2l5TuWz7Bbec67iY4Kvazg> (Date of access: 2/14/2021)].

Summary results of simulations for 1 MJ/m to 243 MJ/m are shown in Figure 2.

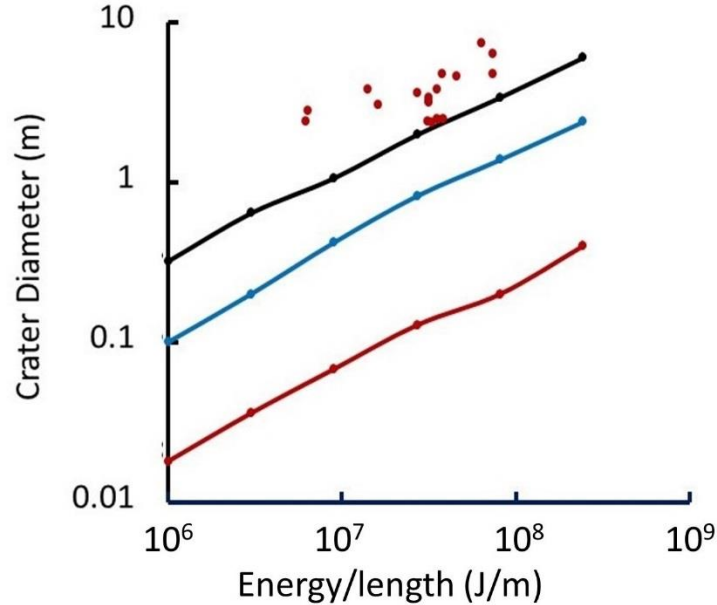


Figure 2. Solid lines show crater diameter in granite (red), clay-sand (blue), and peat (black) as a function of the energy/length from CTH simulations. Data points show the diameter of fractured granite from reference [28].

The central channel in the granite shown in Figure 1 is caused by the compressive pulse which decreases rapidly with increasing distance from the high-energy-density center. When the compressive pulse reflects at the clay-sand boundary, it becomes a tensile pulse and breaks the rock in tension. Since the tensile strength of granite is only $\sim 1.5\%$ of the compressive strength [49], the diameter of fractured granite is much larger than the diameter of the compressed channel [28]. The fracture diameter depends on geometry [29] and composition [28,29] of the explosive, shock impedances of both materials, and distance [28] to material with lower shock impedance. However, those effects are secondary to the main trend, as shown by the scatter in fracture data in Figure 2. Over a wide range of parameters, the fracture diameter from the tensile strain is approximately a factor of 30 larger than the diameter of the channel caused by compressive strain.

3.2 Potential for liquefaction and flow of the clay-sand layer

Peat is ejected into the atmosphere and leaves a crater with smooth sides formed from the shear planes. The granite layer is fractured around the path of an MQN; however, the channel in the fully water-saturated clay-sand of the County Donegal peat bog is very likely to undergo liquefaction and close the channel within tens of seconds after the passage of an MQN.

According to Boulanger and Idriss [30], fine-grained soils, i.e. silts and clays for which the percent of dried soil passing through a No. 200 standard sieve exceeds 50%, require careful testing and analysis to determine whether or not they will undergo liquefaction under an impulse or shaking. Conversely, soils with much less than 50% passing through a No. 200 sieve are much more likely to liquefy when they are saturated with water. We analyzed the clay-sand layer in the County Donegal peat bog and found that it is composed of ~10% rock of ~1 cm diameter, ~20% soil that does not pass a 1 mm screen, and 11% soil passing through a No 200 sieve. Therefore, the fine-grained portion is only ~11% of total mass, or more conservatively, 19% of the sub-mm sized content and well within the < 50% criterion for susceptibility to liquefaction.

Owen and Moretti [31] have identified five conditions that contribute to liquefaction-induced soft-sediment deformation in sands under a transient increase in pore fluid pressure: 1) fine to medium-sized grains of sand, 2) high porosity, 3) high percent saturation with water, 4) low overburden pressure (<10 m of overburden), and 5) no previous liquefaction. The clay-sand layer between the peat and the granite satisfies all five conditions. In addition, Owen and Moretti cite impact by extra-terrestrial objects as a likely trigger for liquefaction. Therefore, we conclude the clay-sand layer is very likely to have undergone liquefaction and obscured the channel within tens of seconds after impact.

3.3 Simulations on circularity of MQN crater as a function of entrance angle

In addition to identifying the signature of MQN impacts, CTH simulations examined the circularity of the crater in the peat bog as a function of entrance angle relative to vertical. The information is helpful in identifying the likely path of the MQN through the liquefied intermediate layer to the bedrock.

Simulations modeled channels at 0°, 15°, 30°, 45°, and 60° to the vertical and between the surface and an immovable solid at 1.0-m depth. The simulated MQN instantaneously deposited 30 MJ/m energy density, as described above. Due to the low strength of the peat, the crater continues to grow for an extended period of time. In order to reasonably simulate the relative effects of the impact angle on the crater dynamics, each simulation was stopped at 10 ms. Figure 3 shows representative profiles.

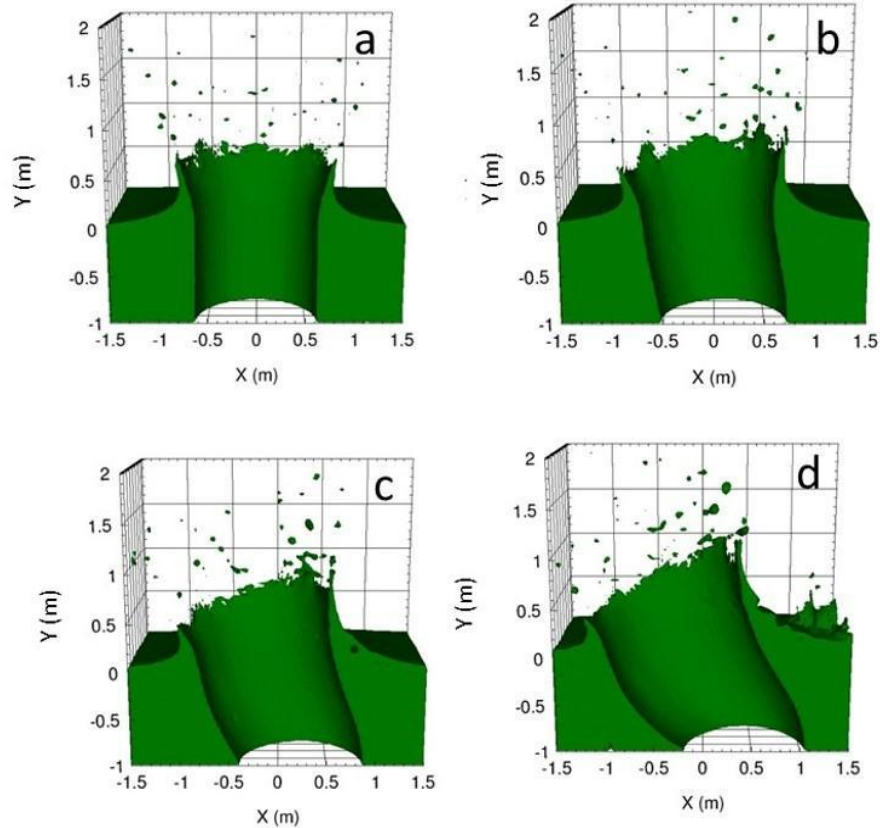


Figure 3. Mass density profiles of peat at $t = 10$ ms after the start of a simulated MQN interaction depositing 30 MJ/m on a trajectory inclined at a) 0° , b) 15° , c) 30° , and d) 45° from the vertical.

At $y = -0.5 \text{ m}$, the ratio of major to minor axes is approximately $\cos^{-1}(\theta)$, as expected for a cylinder intersecting a plane at angle θ . However, Figure 3 shows the peat on the right-hand edges is forced against low-density air while the peat on the opposite side is forced against higher-density peat. The less-impeded peat moves more. Therefore, the asymmetry is enhanced near the rim of the crater. Using the crater shape to estimate θ gives a maximum angle for the trajectory.

3.4 Non-meteorite crater in May 1985 near Glendowan, County Donegal, Ireland

A non-meteorite impact occurred in middle of May of 1985, on Stramore Upper, near Glendowan, County Donegal, Ireland at $54^\circ 58.257' \text{ N}$, $8^\circ 0.408' \text{ W}$. It was reported in the *Donegal People's Press*, May 31, 1985. The article said it occurred “when people were walking their dog”; that would be about 18:00 hours GMT.

The site is on Common Land with rights assigned to a group of nearby landowners, who kindly allowed our research. The National Parks and Wildlife Service has authority over the land and granted us a permit to excavate the site.

Two of us (D. D and S. McG) investigated the crater the day after the event, as part of our duties as Park Rangers. The inside sloped surface of the crater was very smooth. A few-centimeter diameter hole or “pointy” depression was present in the dirt at the center of the crater bottom. There was a distinct, ~2 cm high lip on the peat edge of the crater. Pieces of the bog were scattered up to 10 m away. No meteorite material was ever found.

Figure 4 shows the relatively smooth sides, which are very unusual for craters produced by surface explosives in peat bogs. In addition, large pieces of peat were scattered about 10 m away. The smooth sides, diameter of the crater, and energetically-detached ejecta confirm the fidelity of the CTH simulation.



Figure 4. Photograph of the site soon after the event in 1985 illustrate good agreement in the actual and simulated profile of crater sides.

The crater has a diameter of 3.984 ± 0.065 m in 2006. The yield strength of the peat was measured and found to be 530 ± 120 kN m⁻². Figure 1c and Figure 2 give an energy/meter of ~80 MJ/m for a 4.0-m diameter crater. Uncertainties in the equation of state variables imply a fidelity of +/- 20%.

The shape of the crater was measured in 2006 before it was distorted by investigations. The best fit to an ellipse gives a 1.030 ± 0.005 ratio of major to minor axes and corresponds to $\theta \leq 15^\circ$, as shown in Figure 3a or Figure 3b. The major axis aligned east-west. Therefore, the excavation

was planned to explore the volume within 15° of vertical and optimized for east or west of center.

3.5 Excavations of the 1985 non-meteorite crater in County Donegal, Ireland

Field work a third of the way around the world and in a protected wilderness area is challenging at best. However, it is the least expensive way to test the MQN dark-matter hypothesis. The additional information in Appendix A should assist independent groups in learning from our experiences and re-excavating the site.

The site was excavated in three stages as shown in Figure 5.

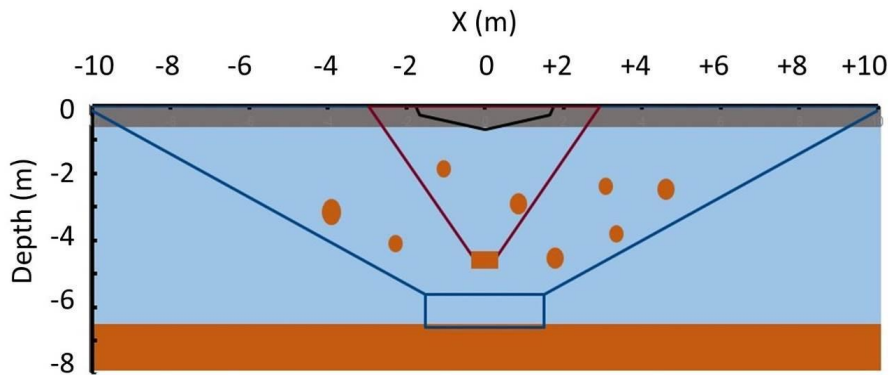


Figure 5. Cross-sectional view of the three excavations: 2017 (black line), 2018 (red line), and 2019 (blue line), and the three layers: peat (gray), clay-sand (blue), and granite (brown). Brown ellipsoids represent the two granite boulders found distributed within the clay-sand volume of the 2018 excavation and the ten found in the 2019 excavation. The brown rectangle shows the location of the only ensemble of fractured rock found in the excavations.

The 2017 expedition excavated the volume defined by the black line in Figure 5 and found that the bottom was composed of compacted clay-sand mixture at depth 0.6 ± 0.1 m. The compacted, post-liquefaction material was too hard to continue excavating by hand.

In 2018, a 6-ton excavator was used in an attempt to reach the bedrock. The volume bounded by the red line in Figure 5 was excavated, with the sides sloping an average of 0.5:1, i.e. 0.5 m horizontal for every 1.0 m vertical, or $\sim 27^\circ$ from vertical, in accord with local experience in this soil. At 4.7 ± 0.1 -m depth, a grouping of fractured rock was discovered just northeast of the center line. After an hour of observing the stability of the sides, the principal investigator was cleared by the civil engineer safety officer to enter the pit. He scooped

accumulated water into a bucket and found the rock was closely packed shards of granite with dimensions varying between 0.02 m and 0.1 m.

The excavation had to be quickly abandoned because the sides of the water-saturated clay-sand mixture showed signs of fracture and sliding at various points down the slope. Since we did not have time to do a careful and well-documented investigation, no samples were removed. The dimension of the rocky bottom was at least the ~0.5 m of the cleared bottom but the horizontal dimension of the rocky area could not be determined; it could be an extensive layer of fractured rock, fractured bedrock, or a localized deposit.

The 2019 expedition used two 14-ton excavators to dig the hole defined by the blue line in Figure 5. The slope of the sides averaged 1.5:1, i.e. 1.5 m horizontal for every 1.0 m vertical, or ~55° from vertical, to assure they would not collapse. Ten boulders were found throughout the excavation. Two of these are shown in Figure 6.



Figure 6. Two of the ten boulders found within the excavated volume are shown. Their diameters are approximately 0.4 m and 0.6 m, and they were distributed throughout the 633 m³ of the 2019 excavation.

Since the material above the rocky grouping of interest had been back-filled after the 2018 excavation, the precise positions of the boulders were not relevant to the 1985 event and were not recorded by the excavator operators.

The operators were requested to excavate to the rocky layer at -4.7 ± 0.1 meters, stop, and alert the team. They did so; however, by the time they stopped and measured the depth, they had removed the volume of fractured rock in just one bucket load, demonstrating that it was a localized deposit, and discharged it through the relocation process to a pile where it spread out. Although they showed us where that load lay, its relational context was lost. We encourage

another group to re-excavate the site and look for fractured granite in the bedrock below our excavation; extreme care is recommended to preserve the context of fractured rock.

Water was pumped from the excavation. The muddy bottom was explored by hand. Rocks shown in Figure 7 were found between 5.0-m and 6.3-m depth. The smaller ones are consistent with those observed at 4.7 m in the 2018 excavation. The larger rocks have slightly rounded edges and may not have been from that grouping.



Figure 7. Granite shards from the volume below the grouping of fractured granite at 4.7 ± 0.1 m are shown. The rocks are covered with the fines from the clay-sand mixture which distorts their natural colors.

These granite rocks were examined with Energy Dispersive Spectroscopy for evidence of large pressure gradients having altered the quartz in the granite. Streaks of darkened mineral was determined to be natural feldspar. No damage attributable to extreme pressures was found.

The excavation continued to a depth of 5.7 m, illustrated by the rectangle outlined in blue in Figure 5. The west face of the crater, just west of the grouping of shards found in 2018, was washed with a pressure washer to better reveal its composition. A photo of the washed face is shown in Figure 8.



Figure 8. Pressure-washed face of the excavation's west side, adjacent to the grouping of shards at the 4.7 ± 0.1 m depth found in the 2018 excavation.

Figure 8 shows no evidence of a horizontal layer of shards or bedrock, demonstrating that the ensemble of fractured granite was an isolated one, approximately the size of a shattered boulder. This group of shards was in the projected path of the impactor and was the only such grouping found in the excavation. Since boulders closer to the surface but outside the projected path were not shattered, we conclude that the ensemble of fractured granite was not shattered by pressure waves originating from energy deposited near the surface.

The decrease of pressure with increasing distance in the movies of the CTH simulations in Supplementary Material and the diameter of the fractured granite in Figure 2 indicates that a direct hit by an MQN may be required, and would be sufficient, to fracture a whole boulder. If so, and if the boulders were randomly distributed within the excavated volume, the probability of even one boulder being intercepted and fractured was only $\sim 7\%$. Consequently, it is not surprising that only one collection of shards was found and that it was well within the projected path of the penetrator. Therefore, we infer the hypervelocity object shattered the granite boulder after passing through 0.7 m of peat and 3.9 m water-saturated soft sediments.

As shown in Figure 9, we found at ~ 6.3 -m depth, irregular boulders and large flat slabs of granite, with the vector normal to a slab inclined at $\sim 30^\circ$ to the vertical on the south, $\sim 60^\circ$ to the vertical on the north, and $\sim 90^\circ$ to the vertical in the middle. We did not find a uniform slab of bedrock that would have been a perfect witness plate of a quark-nugget passage by showing a cylinder of fractured granite extending into the earth. Since our simulations give ~ 160 MJ/m (the equivalent of ~ 160 sticks of dynamite per meter) in granite to match the crater, broken slabs in disarray might be expected.

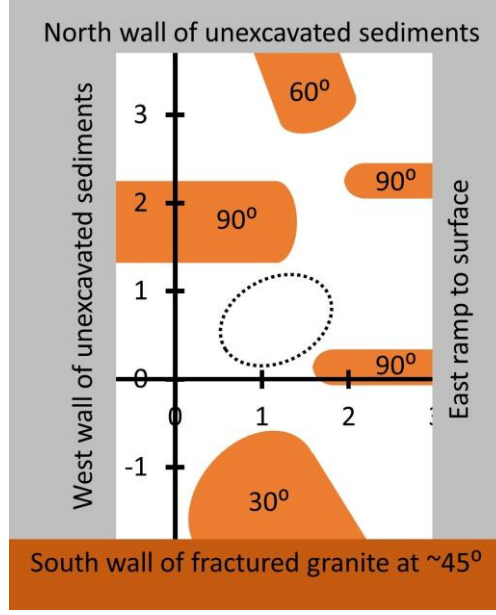


Figure 9. Layout of granite rocks (brown) and sediment walls (gray) at depth of ~ 6.3 to 6.5 m. The scale is in meters and the angles are between the vertical and the normal to the largest-area surface. The origin is directly below the center of the original impact crater on the surface with an estimated accuracy of ± 0.3 m. The dotted ellipse shows the approximate projection of the shattered rock found in the 2018 excavation at 4.7 -m depth to the 6.4 -m depth shown here.

We could not determine if the mixture of rocks and slabs at different angles to the horizontal, shown in Figure 9, were characteristic of the site before the 1985 event or were caused by that event. Additional excavation directly beneath the grouping of fractured rock at ~ 4.7 -m depth was blocked by large boulders or displaced slabs around that volume. These obstacles were too large to move with available equipment. In addition, the excavation from 4.8 m to 6.3 m had nearly vertical walls, which introduced a safety risk and precluded more excavation within the limitations of the project.

3.6 Potential for independent validation of the 1985 event

The force equation for a high-velocity body with instantaneous radius r_m , mass m , and velocity v , moving through a fluid of density ρ_p with a drag coefficient $K \approx 1$ is

$$F_e \approx K\pi r_m^2 \rho_p v^2. \quad (1)$$

MQNs have a velocity-dependent interaction radius [23] equal to the radius of their magnetopause

$$r_m \approx \left(\frac{2B_o^2 r_{QN}^6}{\mu_0 K \rho_p v^2} \right)^{\frac{1}{6}}, \quad (2)$$

in which r_{QN} is the radius of the MQN of mass m and mass density ρ_{QN} :

$$r_{QN} = \left(\frac{3m}{4\pi\rho_{QN}} \right)^{\frac{1}{3}}. \quad (3)$$

The interaction radius of an MQN varies as velocity $v^{-1/3}$ in equation (2). Including that velocity dependence in the calculation with initial velocity v_o gives velocity as a function of depth x yields

$$v = v_o \left(1 - \frac{x}{x_{\max}} \right)^{\frac{3}{2}}, \quad (4)$$

in which x_{\max} is the stopping distance for an MQN:

$$x_{\max} = \left(\frac{3m}{2\pi r_{QN}^2} \right) \left(\frac{\mu_o v_o^2}{2K^2 \rho_p^2 B_o^2} \right)^{\frac{1}{3}}. \quad (5)$$

The ~10 kg MQN inferred for the 1985 crater penetrates to $x_{\max} = 3572$ m for $\rho_p = 2020$ kg/m³.

Since we only explored the 1985 event to a depth of 6.5 m, it is possible for an independent team to re-excavate the site of the 1985 event to the bedrock and look for an extended volume of fractured granite. We marked the site to facilitate such an independent examination.

3.7 Additional limit on B_o to $\geq 4 \times 10^{11}$ T

Comparing simulation results with observations from the crater implies the crater was formed with 80 +/- 16 MJ/m energy deposition in the peat. The MQN mass that can deposit that energy density and the corresponding number of events per year were computed as a function of B_o [15]. Table 1 summarizes the results to compare with observations.

Table 1: Maximum mass, mass capable of delivering 80 MJ/m and 1 kJ/m, and an estimate of the corresponding event rates for interstellar dark-matter mass density $\sim 7 \times 10^{-22}$ kg/m³ [1,53] and 250 km/s impact velocity, the relative velocity of the solar system through the dark matter halo. NA = Not Applicable and means there was no solution.

B_o (TT)	Maximum Mass (kg)	Mass of MQNs depositing ~80 MJ/m (kg)	Expected events/y on Earth capable of ~ 80 MJ/m	Mass of MQNs depositing >1 kJ/m (kg)	Expected events/y depositing > 1 kJ/m	Ratio of rate > 1 KJ to rate ~ 80 MJ/m

0.1	7×10^{-3}	NA	0	7×10^{-6}	100,000,000	NA
0.2	2×10^{-1}	NA	0	2×10^{-5}	3,000,000	NA
0.3	3	NA	0	4×10^{-5}	800,000	NA
0.4	2×10^1	16.9	2,000	5×10^{-5}	600,000	350
0.5	1×10^2	13.9	3,000	8×10^{-5}	200,000	50
0.6	1×10^2	11.8	3,000	1×10^{-4}	50,000	20
0.7	7×10^2	10.3	900	1×10^{-4}	20,000	30
0.8	1×10^3	9.1	300	2×10^{-4}	20,000	50
0.9	7×10^3	8.2	20	2×10^{-4}	1,000	50
1.0	2×10^4	7.5	20	2×10^{-4}	1,000	60
1.1	4×10^4	6.9	20	2×10^{-4}	900	50
1.2	1×10^5	6.4	40	3×10^{-4}	200	60
1.3	1×10^5	5.9	20	3×10^{-4}	100	50
1.4	6×10^5	5.6	30	4×10^{-4}	100	40
1.5	7×10^5	5.2	20	4×10^{-4}	90	40
1.6	1×10^6	4.9	0.9	4×10^{-4}	20	30
1.7	3×10^6	4.7	0.4	5×10^{-4}	10	30
1.9	6×10^6	4.2	0.3	6×10^{-4}	10	30
2.0	9×10^6	4.0	0.2	6×10^{-4}	7	30
2.1	1×10^7	3.9	0.5	7×10^{-4}	2	30
2.3	5×10^7	3.6	0.06	8×10^{-4}	2	30
2.4	2×10^8	3.4	0.06	8×10^{-4}	0.4	10
2.6	2×10^8	3.2	0.003	9×10^{-4}	0.2	10
2.8	6×10^8	3.0	0.003	1×10^{-3}	0.2	10
3.0	1×10^9	2.8	0.005	1×10^{-3}	0.03	10

3.1	2×10^9	2.7	0.0003	1×10^{-3}	0.02	10
10.0	8×10^{14}	1.0	3×10^{-8}	7×10^{-3}	2×10^{-7}	10

Table 1 shows the MQN mass necessary to deposit 80 MJ/m in water-saturated peat as a function of B_o . Since the maximum MQN mass in distributions with $B_o < 4 \times 10^{11}$ T cannot deliver that energy deposition, we exclude $B_o < 4 \times 10^{11}$ T.

The last column in Table 1 gives the ratio of event rate with enough energy deposition (~ 1 kJ/m) to leave some geophysical evidence to the event rate sufficient to produce the crater in 1985 (~ 80 MJ/m). The ratio varies from 10 to 350 for the allowed range of B_o and indicates there could be a sufficient number of events to study, if they can be identified and if access to the sites can be obtained.

3.8 Event rate of non-meteorite cratering events and duplicative constraint on B_o

In addition to comparisons by MQN mass, an observed event rate can be compared to theoretical predictions of event rate in Table 1. Three non-meteorite events in three years were cited in the Introduction. Estimated energy/meter deposited from Figure 2 above and the MQN mass from Figure 2 of reference [15] for the 2016 event in Tamil, India that killed a man was ~ 80 MJ/m, which is comparable to the energy deposition in the County Donegal event. The 2015 event in Rhode Island, USA, is consistent with ~ 1 kJ/m energy deposition. The 2014 event in Managua, Nicaragua, is consistent with ~ 30 GJ/m deposited in soft sediment. The approximately annual event rate can be associated with MQN impacts delivering ≥ 1 kJ/m. Table 1 summarizes the event rate for that mass range as a function of B_o . An annual event rate appears to exclude $B_o > 2.3 \times 10^{12}$ T.

However, we need to interpret these results cautiously. We do not know what fraction of all events are observed and reported. If that fraction is small, then some values of $B_o \leq 2.3 \times 10^{12}$ T would also be excluded. On the other hand, MQNs can certainly survive transit through a portion of the solar chromosphere and photosphere and be decelerated (by the MQN magnetopause interaction with solar plasma) to less than escape velocity from the solar system. A very small fraction of these trapped MQNs can receive sufficient angular momentum, by subsequent interaction with a planet, so that they are not absorbed into the sun. In principle, these captured MQNs can accumulate and enhance the dark-matter density inside the solar system, compared to that of interstellar space. Our preliminary estimates give an enhancement factor of ~ 300 . Until adequate simulations of this aerocapture process are completed, we refrain from excluding B_o values compatible with an enhancement of 300. Therefore, the upper excluded value based on event rate remains $B_o > 2 \times 10^{12}$ T and is less restrictive than the constraint based on MQN mass in section 3.7.

4. Discussion

4.1 Consistency with MQN Impact

Five points of agreement between theory, as interpreted by the simulations, and data from the three witness-plate layers combine to provide the second of many needed observations consistent with MQN dark matter.

1. The 4-m diameter crater is consistent with CTH simulations of ~80 MJ/m energy deposition. That energy/length is consistent with a 10 +/- 7 kg MQN with $4 \times 10^{11} T \leq B_0 \leq 3 \times 10^{12} T$. It is not consistent with a meteorite because no meteorite material was found and because the crater diameter is much too small to be within the range of meteorite craters. Meteorites must be either very aerodynamically shaped, which is very unlikely, or be at least ~ 20-m diameter to be large enough to survive transit through the atmosphere [24]. Meteorite craters are typically an order of magnitude larger in diameter than the meteorites that make them, so meteorites are usually found in craters with diameter ~200 m or larger. The smallest diameter crater associated with a meteorite in the last century impacted in 2007 at Caranacas, Peru. It was 13.5-m diameter. The crater was at an altitude of 3,500 m. Its small diameter may be attributed to its not having to survive the densest part of the atmosphere. As noted in the Introduction, non-meteorite craters are reported in the press approximately annually and are less than 12-m diameter. The lack of overlapping size and event rate suggests craters like the one studied in this paper must be caused by a phenomenon other than a meteorite.
2. The CTH simulations show the crater sides are formed by shear-planes and are smooth, as independently reported by the two Rangers investigating the day after the event. We found that smooth sides are in stark contrast to the irregular sides of craters produced by large explosives on the surface of the peat bog, so smooth crater sides are a distinguishing point of comparison.
3. The CTH simulations show that chunks of ejecta have sufficient velocity to be thrown clear of the site. Rangers reported the ejecta landed ≥ 10 m from the crater. The photograph in Figure 4 shows no ejecta near the crater, which confirms their report.
4. The “pointy depression” at the center of the crater bottom is consistent with the computed channel through the soft sediments and subsequent flow of material. Since the water-saturated soft sediments below the peat met all the requirements for liquefaction [30] by the impact, the soft sediments must have liquefied and flowed back into the void to refill the central channel shown in Figure 2. Refilling would have occurred from the bottom, where the pressure from the overburden is greatest, to the top. When the overburden pressure becomes too small to overcome viscosity, a “pointy” depression should remain, as observed on the day following the impact.
5. A volume of shattered granite was found only at 4.7-m depth and within the projected impact trajectory at 15° from vertical. All 10 boulders found outside the trajectory were intact. The uniqueness of the shattered granite and its location indicates the hypervelocity body that caused the crater in the peat layer also shattered the granite boulder at 4.7-m depth. Passage through the 0.7-m peat layer and 4.0-m soft-sediment layer with sufficient residual velocity to shatter the granite requires material strength that is much greater than the material strength of normal matter. The electromagnetic force holds together normal matter. The strong nuclear force is the only alternative. It

holds together quark nuggets. Strong-force material strength, the corresponding nuclear mass density, and energy deposition in the MJ/m range in solid density matter are uniquely consistent with quark nuggets. Therefore, hypervelocity penetration through many meters or kilometers of solid or liquid density normal matter and energy deposition in the MJ/m range are a unique signature of an MQN. The deeply buried and shattered granite is, therefore, consistent with an MQN impact.

4.2 Probability of fractured granite attributable to the impactor that made the 1985 crater

The fifth point of comparison in section 4.1 assumes that the fractured-granite deposit was caused by the impactor that produced the crater. We found only one fractured-granite deposit in the 633 m³ excavation. It was at 4.7-m depth and within the calculated trajectory of the crater-forming impactor. As with all non-meteorite impacts, the state of subsurface rock before the 1985 impact is uncertain. Consequently, we cannot be certain that the highly localized and uniquely fractured granite was not fractured before the impact. Its association with the impact is based only on its location and uniqueness.

The null hypothesis is that the fractured granite at 4.7-m depth and the crater on the surface were not caused by the same event. If the probability of the null hypothesis is < 0.05 , then the results are usually considered worthy of further investigation as possible evidence for a new phenomenon. We estimate the probability P_{null} that the null hypothesis is true. P_{null} has two factors:

1. P_1 = probability of the single shattered boulder being randomly located within the effective range R_{eff} of the impactor trajectory for fracturing granite. $P_1 = \text{volume_ratio} = \pi R_{eff}^2 L / (633 \text{ m}^3 \text{ volume of excavation})$, where $L \sim 5 \text{ m}$ depth of excavation
2. P_2 = probability of 10 intact boulders being outside the effective range R_{eff} . Since the probability that one boulder is outside R_{eff} is $1 - \text{the probability it is inside } R_{eff}$ and since all 10 are assumed to be independently located, $P_2 = (1 - \text{volume_ratio})^{10}$.

Therefore, $P_{null} = (0.025 R_{eff}^2) \times (1 - 0.025 R_{eff}^2)^{10}$.

Figure 9 shows the impactor trajectory is within 1 meter of granite slabs that are still intact, so $R_{eff} \leq 1 \text{ m}$ if energy deposition in the clay is effective in fracturing granite. As summarized in section 3.1 from references [28,29], granite fractures from the tensile stress after compression waves that originate inside the granite reflect off of the interface with lower-impedance media. If fracturing into shards requires energy directly deposited inside the granite, then $R_{eff} \leq 0.45 \text{ m}$, the boulders' mean diameter. The two estimates of R_{eff} give probability P_{null} between 0.005 to 0.02. Since we did not measure the exact location of each boulder as it was excavated, the P_2 term is less certain but is not sensitive to this number. Setting the less certain P_2 term to 1, still gives P_{null} between 0.005 to 0.025. The probability that the fractured boulder is associated with the impact is $1.0 - P_{null}$ is $>98\%$. The high probability of association supports the consistency of the 1985 event with an MQN impact.

4.3 Less than 20-m diameter craters are incompatible with normal-matter impactors.

The 80 MJ/m deposited in the 1985 event requires the impactor to have been a hypervelocity body, which generally refers to velocities $> 3,000$ m/s and to impacts in which material strength is much less than internal stresses. Hydrodynamic simulations [24] of the Shoemaker–Levy 9 comet (D/1993 F2) provided theoretical results to compare with the first direct observation of a hypervelocity extraterrestrial object colliding with an atmosphere. The aerodynamic force, proportional to atmospheric density times the square of the velocity, causes it to decelerate and produces a strong shock wave in front of it. The interaction compresses, heats, and ionizes atmospheric gas. Plasma temperatures can reach 25,000–30,000 K. Associated thermal radiation is absorbed by the surface material of the impactor and causes rapid ablation and vaporization. Usually, the body completely ablates into meteoritic vapor or breaks into many small fragments that quickly slow to subsonic terminal velocity. This effect is consistent with meteorites distributed over a wide area without a crater, as observed in Antarctica, since these small meteorites are from the breakup of meteors in the atmosphere.

If the meteor is sufficiently large and sufficiently aerodynamic, it reaches the ground intact with a significant fraction of its mass and is still moving at hypervelocity speeds. It then produces an impact crater accompanied by meteorite material at the impact site. The dynamics associated with passage through Earth's atmosphere assures zero to a very small fraction of meteors with < 20 -m diameter survive and maintain sufficient speed to cause an impact crater [24]. Since the diameter of an impact crater is typically $\sim 5\%$ the diameter of the impactor, impact craters less than ~ 100 m in diameter are inconsistent with normal-matter impactors. Therefore, the 3.5-m diameter crater from the 1985 event is inconsistent with normal-matter impactor.

4.4 Normal-matter impactors delivering the inferred energy to the peat are incompatible with shattering granite 4.7 m below the surface.

The impactor in the 1985 event delivered ~ 80 MJ/m to the 0.7 m of peat, penetrated 4.0 m of water-saturated soft sediments, and still had enough momentum to shatter the granite boulder with an observed diameter ≥ 0.6 m. Any MQN that deposits ~ 80 MJ/m in the peat will also deposit, proportional to its mass density, ~ 160 MJ/m in the granite. This is well in excess of the ~ 1 MJ/m required in granite to shatter the boulder, as shown in Figure 2.

Transit through solid or liquid density media would require surviving dynamic forces more than 1000 times those experienced in the atmosphere and discussed in section 4.3, so such transits are prohibited for normal matter. In addition, conservation of linear momentum assures an approximately spherical body (not a long rod penetrator) is decelerated with an e-folding distance of approximately its diameter times the ratio of impactor density to media density. Meteorites typically make a crater about 20 times the meteor diameter. Even if the impactor is not vaporized upon impact, a normal-matter impactor would lose most of its velocity within a few tenths of the crater diameter. Consequently, we can rule out normal-matter impactors as the cause of shattered granite boulders that are 4.7 m below the 3.5-m diameter crater in Ireland.

However, the material strength of an MQN is determined by the strong nuclear force. They are indestructible in interactions at even 250 km/s. The corresponding mass density is nuclear density $> 7 \times 10^{17} \text{ kg/m}^3$ and this assures that their momentum will let them penetrate many meters or even kilometers into Earth, as discussed in section 3.6.

4.5 Alternative explanations

Quark nuggets, neutronium, and black holes have mass densities greater than the required value. However, neutronium is not stable outside of neutron stars, and black holes small enough to provide the local density of dark matter and provide at least one impact per year reported in the press, i.e. $\sim 10 \text{ kg}$ mass, would have evaporated in about 150 y, which is much shorter than the time over which the effects of dark matter have been stable. Therefore, crater formation by quark-nugget impact is the only explanation that fits the data and is consistent with established physics.

4.6 Limitations to evidence and need for systematic study

The 1985 impact is only the second reported event consistent with the MQN hypothesis. Many more are needed to conclude that MQNs exist. The three non-meteorite events cited in the Introduction could be investigated as additional quark-nugget events. Additional candidates are listed in Supplementary Results: Additional candidate sites for MQN impacts in County Donegal. However, the dates of these potential events are unknown, and there may be competing processes for producing crater-like holes in otherwise flat peat bogs. Gaining physical and administrative access to investigate these additional sites may be difficult. Our investigation of the 1985 impact in Ireland required fifteen years even with a supportive local community and national authority.

Additional and independent excavation of the 1985 event in County Donegal is lower risk and could independently confirm or invalidate our result by determining if the bedrock shows the expected cylindrical hole of fractured granite with radius of fracture decreasing with increasing depth. In addition, the expedition could determine if the tilted granite slabs and granite rocks at 6.3-m depth are a universal feature of the bedrock in the area or were caused by the 1985 event. The latter case would provide additional evidence of large and local energy deposition at depth. The information in Appendix A should be helpful to such an expedition.

Even with additional evidence from non-meteorite craters, a systematic study is necessary. Obtaining the results in this paper required fifteen years, including the time to obtain permission to excavate from supportive land owners and Irish national authorities. Although such events apparently occur annually on Earth, obtaining permission and excavating each one is impractical. If remote acoustic sensing [32] of the subsurface interface between granite bedrock and soft sediments could be further developed to provide a profile on the interface with $\sim 10\text{-cm}$ resolution through $\sim 10 \text{ m}$ of soft sediments, then the pattern shown in Figure 9

might be identified as uniquely associated with the impact event. If so, new events could be explored if access to the site can be secured. In addition, the rest of the peat bog in county Donegal could be non-destructively mapped to identify additional sites that occurred over the last 3500 years. Appendix B has a list of candidate sites for MQN impacts in County Donegal. With this method, a statistically significant set of data might be obtainable.

Whether or not such a technology can be developed, the event reported in this paper motivates developing and deploying a constellation of three satellites at 51,000 km altitude to look for RF signatures of MQNs after they transit the magnetosphere [45]. Such a space-based system would provide real-time search for MQNs based on their predicted Doppler-shifted-radiofrequency signature and is the best approach for the necessary and systematic study of the MQN hypothesis for dark matter.

5. Conclusions

We report computer simulations of the MQN energy deposition in water-saturated peat, soft sediments, and granite and report results from excavating such a crater. The >98% probability that the fractured boulder is associated with the impact (section 4.2) and the five points of agreement between the simulation results and the observations (section 4.1) support the inference that the 1985 event is consistent with an MQN impact. This is the second event found to be consistent with MQNs. The first is described in reference [17]. However, many additional non-meteorite impacts with a similar effect on deeply buried rock and/or additional tests that stress different aspects of the MQN hypothesis are needed to conclude whether or not MQNs exist and contribute to dark matter. The results also redundantly constrain B_0 to $\geq 4 \times 10^{11}$ T, which is consistent with the previously published most likely values of $B_0 = 1.65 \times 10^{12}$ T +/- 21%.

Supplementary Materials: Movies of pressure, mass density, and temperature from the CTH simulations available at VanDevender, J. Pace; Schmitt, Robert; Simulations of magnetized quark nugget dark matter in three-layer witness plate, Dryad, Dataset, 2020, <https://doi.org/10.5061/dryad.cc2fqz641>.

Author Contributions: Conceptualization, Aaron VanDevender; Data curation, J. Pace VanDevender and Niall McGinley; Formal analysis, J. Pace VanDevender and Robert G. Schmitt; Funding acquisition, J. Pace VanDevender; Investigation, J. Pace VanDevender, Robert G. Schmitt, Niall McGinley, David G. Duggan, Seamus McGinty, Aaron VanDevender, Peter Wilson, Deborah Dixon, Helen Girard and Jacquelyn McRae; Methodology, J. Pace VanDevender, Robert G. Schmitt, Niall McGinley, Aaron VanDevender and Peter Wilson; Project administration, J. Pace VanDevender; Resources, J. Pace VanDevender; Software, Robert G. Schmitt; Supervision, J. Pace VanDevender; Validation, Robert G. Schmitt and Aaron VanDevender; Visualization, Robert G. Schmitt; Writing – review & editing, Robert G. Schmitt, Niall McGinley, David G. Duggan, Seamus McGinty, Aaron VanDevender, Peter Wilson, Deborah Dixon and Helen Girard.

All authors have read and agreed to the published version of the manuscript.

Funding: This research was primarily funded by VanDevender Enterprises and volunteers. In addition, New Mexico Small Business Assistance to Sandia National Laboratories funded the CTH hydrodynamic simulations.

Institutional Review Board Statement: Not applicable

Informed Consent Statement: Not applicable

Data Availability Statement: All final analyzed data generated during this study are included in this published article and associated supplementary information.

Acknowledgments: We gratefully acknowledge S. V. Greene for first suggesting we consider quark nuggets and Mark Boslough for critical review and suggestions. Ranger David Dugan provided greatly appreciated guidance and assistance in obtaining the necessary permit from the National Parks and Wildlife Service. Mr. Charlie Callahan of Glendowan provided essential guidance and assistance from the point of view of local residents with rights to use this land. Mr. Cathal Moy and his associates were invaluable; without their knowledge of local soil conditions and exceptional skill with operating their excavators, the project could not have been accomplished. Volunteers Rebecca Stair and Nathan Girard assisted in the 2018 and 2019 excavations respectively. Finally, Jesse A. Rosen edited this paper and improved the structure, logic, and flow.

This work was supported by VanDevender Enterprises, LLC. The CTH simulations were supported by the New Mexico Small Business Assistance (NMSBA) Program through Sandia National Laboratories, a multi-program laboratory operated by National Technology and Engineering Solutions of Sandia (NTESS), a wholly owned subsidiary of Honeywell International, with support from Northrup Grumman, Universities Research Association and others., for the U.S. Department of Energy's National Nuclear Security Administration. By policy, work performed by Sandia National Laboratories for the private sector does not constitute endorsement of any commercial product.

Conflicts of Interest: The authors declare no conflict of interest.

Appendix A. Excavations

To assist another team to extend the excavation into the bedrock and independently test and extend our findings, the three excavations are described in this section. Please check the Acknowledgements for the names of essential team members from County Donegal.

The 2017 expedition cleared out debris and plant growth by hand. The bottom, at depth -0.6 ± 0.1 m, was compacted clay-sand mixture.

The 2018 expedition employed a single Hitachi EX-60, 6-ton excavator shown in Figure A1 with the 4-m diameter crater drained by the channel on the right edge. The site was excavated with the sides sloping at 27° to the vertical, in accord with local experience in this soil. However, the excavation had to be quickly abandoned because the sides of the water-saturated clay-sand mixture showed signs of fracture and sliding at various points down the 27° slope.



Figure A1. View of the 4-m diameter crater from 1985, drained with a channel shown to the down sloping terrain on the right.

The 2019 expedition employed two Doosan 140LC, 14-ton excavators. One was on a ramp inside the excavation and moving material to the surface. The second excavator relocated each scoop of material to a safe distance from the hole to avoid increasing pressure on the soil adjacent to the hole and provide a flat surface for the second excavator to traverse. The slope of the sides was approximately 55° from vertical as shown in Figure A2. That slope held.



Figure A2. Excavation in 2019 to depth of 5.7 m and showing access ramp, submersible water pump and hose, and exit ladder. Examining the bottom and recovering rock fragments had to be done by feel at this stage.

An additional 1.5 m of material, plus a water-collecting hole for the submersible pump, was excavated to look for bedrock. From 4.8-m to 6.3-m depth, we found irregular boulders, smaller rocks, and large flat slabs of granite with their normal vector inclined at 30° to the vertical on the south side, and 60° to the vertical on the north, as shown in Figure A3.



Figure A3. Photo of the collection of granite rocks found at approximately 6.3-m depth to the southeast of the center of the crater. The normal to the slab on the right is inclined at 30° to the vertical.

We did not find a uniform slab of bedrock and could not determine if the mixture of rocks and slabs at different angles to the horizontal were characteristic of the site before the 1985 event or were caused by that event. Additional excavation directly beneath the grouping of fractured rock at ~4.5-m to ~4.8-m depth was blocked by two large boulders or displaced slabs to either side of that volume. These obstacles were too large to move with available equipment. In addition, the excavation from 4.8 m to 6.3 m had nearly vertical walls, which introduced a safety risk that precluded more excavation within the limitations of the project.

If another group re-excavates the site to examine the bedrock and search for the signature of MQN passage, i.e. a cylinder of fractured granite extending well into the earth, extreme care is recommended below the 6.3-m depth to preserve the context of fractured rock.

In accord with our permit, the site was first filled with the rock and clay-sand mixture and topped with the peat layer. A wooden pole was driven into the peat to mark the center of the original 1985 impact crater. Three orange plastic stakes are located on elevated mounds at 1) 21.9 m to the south, 2) 26.76 m to the west, and 3) at 40.12 m at 61.5° north of west. Surveyor's lines from each stake connect the stake to the center post in hopes that another expedition could easily find and re-excavate the site.



Figure A4. Wooden stake and three survey lines mark the center of the original impact crater for subsequent expeditions to extend the investigation into the granite bedrock below 6.5-m depth.

Appendix B: Additional candidate sites for MQN impacts in County Donegal

In 2006, we conducted an aerial survey of about 600 km² of peat bog to look for other evidence of deformations from massive objects. We found at least two additional holes and inspected them on the ground: 1) approximately 4-m by 5-m diameter and 2 m deep at 54° 55.362' N and 8° 15.260' W and 2) approximately 4.8-m by 5.1-m diameter and 2.1 m deep at 54° 55.434' N and 8° 15.002' W. Since no one reported witnessing their being formed, we could not confirm that they were associated with impacts.

Since the aerial search in 2006, the resolution in the Google maps covering the western portion of the peat bog has been improved to the point that the maps are useful for a survey. Water flowing below the peat can create multiple holes aligned along the flow in peat bogs. Other mechanisms may also produce holes. Therefore, a survey of isolated round holes, like the 1985 event but without eye witnesses, will only give an upper limit to the event rate. A survey that was informed by the examination of the two holes found in 2006 was conducted in 2014. The survey consisted of 200 randomly selected areas in a square defined by the GPS coordinates of the opposing corners (54.918855, -8.222008) and (54.977614, -8.421822). The chosen area had adequate resolution and did not include any human structures. It was a peat bog with reeds growing on top of the older peat. The total area surveyed in the 200 samples was 3 km². The

survey identified 33 circular depressions like the two we qualified in the ground-based survey. The 33 positions are shown in Table A1.

Table A1: Coordinates and description of deformations in peat-bog survey

GPS Coordinates	Diameter	Description
54.920869,-8.398206	6m ± 2m	very circular, more faded than other shapes
54.921385,-8.296381	6m ± 2m	circular, lighter strip running through circle
54.926524,-8.310256	6m ± 2m	circular, faded, extension from bottom right of circle
54.927851, -8.34372	4m ± 2m	very circular, more faded than other shapes
54.929398,-8.261827	3m ± 2m	circular, nodule on top right and left of circle
54.931636,-8.270241	2m ± 1m	circular, little nodule on top right of circle
54.931716,-8.225976	4m ± 2m	circular, dip on bottom right of circle
54.93359,-8.355017	4m ± 2m	circular, tiny dip at top left corner, surrounded by white
54.935795,-8.269017	3m ± 2m	circular, sort of flat on top and bottom
54.93674,-8.265257	2m ± 1m	very circular, surrounded by white
54.937784,-8.267118	3m ± 2m	circular, nodule on top left of circle
54.938974,-8.274889	4m ± 2m	circular, dip on top left of circle
54.939262,-8.267507	4m ± 2m	circular, diagonal oval shape
54.940387,-8.322002	3m ± 2m	very circular, more faded than other shapes
54.942222,-8.319636	4m ± 2m	circular, white in center of circle
54.943955,-8.276018	2m ± 1m	very circular, surrounded by white
54.944405,-8.278464	2m ± 1m	very circular, surrounded by white
54.946506,-8.292173	2m ± 1m	very circular, small
54.947903,-8.23144	6m ± 2m	circular, two small rounded extensions at bottom
54.949308,-8.399971	4m ± 2m	circular, nodule on bottom left of circle
54.949494,-8.298809	5m ± 2m	circular, upright oval looking, faded
54.951723,-8.30839	5m ± 2m	circular, diagonal oval shape
54.95572,-8.265512	3m ± 2m	circular, slightly greater width than height

54.956526,-8.24444	3m ± 2m	circular, small dip on bottom of circle
54.962613,-8.273741	1m ± 0.5m	circular, tiny nodule on right side of circle
54.964019,-8.305927	4m ± 2m	very circular, more faded than other shapes
54.964546,-8.269087	2m ± 1m	circular, slightly greater height than width
54.964943,-8.235828	2m ± 1m	very circular, more faded than other shapes
54.965639,-8.237676	5m ± 2m	circular, nodule on bottom right of circle
54.969051,-8.261765	3m ± 2m	circular, bit cut off bottom right of circle
54.969271,-8.277284	3m ± 2m	circular, nodule on top right of circle
54.970346,-8.377996	1m ± 0.5m	circular, diagonal oval shape
54.971057,-8.320993	3m ± 2m	circular, extension from bottom of circle

Poisson statistics gives a 95% confidence for an upper limit of 11 ± 3.7 events per km^2 . Their diameters ranged from 2 ± 1 m to 9 ± 2 m. The crater from the 1985 event has changed little in 33 years and should last at least 100 years under the same environmental stresses. The extrema of 100 and 200 years for the time period give an estimated event rate of 0.1 to 0.05 events/ km^2/yr . Since the area of the earth is $\sim 5 \times 10^8$ km^2 , the corresponding global event rate is between 30×10^6 and 60×10^6 events per year. Such a large number of potential events illustrates the likelihood of other phenomena forming holes in peat bogs and the importance of eyewitnesses to impacts.

References

1. Aghanim, N. *et al.* (Planck Collaboration), Planck 2018 results. VI. Cosmological parameters. Available online: <https://arxiv.org/pdf/1807.06209.pdf>. (accessed on 2/14/2021).
2. Peebles, P. J. E. *Cosmology's Century, an inside story of our modern understanding of the universe*; Princeton University Press: Princeton, NJ, USA, 2020; 216-297.
3. Iocco, F.; Pato, M.; Bertone, G. Evidence for dark matter in the inner Milky Way. *Nat. Phys.* **2015**, *11*, 245-248. <https://doi.org/10.1038/nphys3237>
4. Steinmetz, M.; Navarro, J. F. The hierarchical origin of galaxy morphologies. *New Astron.* **2002**, *7*, 155-160. [https://doi.org/10.1016/S1384-1076\(02\)00102-1](https://doi.org/10.1016/S1384-1076(02)00102-1)
5. Douglas, C. *et al.* A direct empirical proof of the existence of dark matter. *Astrophys. J.* **2006**, *648*, L109-L113. <https://doi.org/10.1086/508162>
6. Salucci, P. The distribution of dark matter in galaxies. *Astron Astrophys Rev* **2019**, *27*, 2. <https://doi.org/10.1007/s00159-018-0113-1>
7. Patrignani, C., *et al.* Review of particle properties (Particle Data Group) *Chin. Phys.* **2016**, *C40*, 100001. <https://doi.org/10.1088/1674-1137/40/10/100001>
8. Witten, E. Cosmic separation of phases. *Phys. Rev. D* **1984**, *30*, 272-285. <https://doi.org/10.1103/PhysRevD.30.272>
9. Farhi, E.; Jaffe, R. L. Strange matter. *Phys. Rev. D* **1984**, *30*, 2379-2391. <https://doi.org/10.1103/PhysRevD.30.2379>

10. De Rújula, A.; Glashow, S. L. Nuclearites—a novel form of cosmic radiation. *Nature* **1984**, *312*, 734-737. <https://doi.org/10.1038/312734a0>
11. Zhitnitsky, A. "Non-baryonic" dark matter as baryonic color superconductor. *JCAP* **2003**, *0310*, 010. <https://doi.org/10.1088/1475-7516/2003/10/010>
12. Xia, C. J.; Peng, G. X.; Zhao, E. G. ; and Zhou, S. G. From strangelets to strange stars: a unified description. *Sci. Bull.* **2016**, *61*, 172. <https://doi.org/10.1007/s11434-015-0982-x>
13. Jacobs, D. M.; Starkman, G. D.; Lynn, B. W. Macro dark matter. *MNRAS* **2015**, *450*, 3418–3430. <https://doi.org/10.1093/mnras/stv774>
14. Burdin, S., *et al.* Non-collider searches for stable massive particles. *Phys. Rep.* **2015**, *582*, 1-52. <https://doi.org/10.1016/j.physrep.2015.03.004>
15. VanDevender, J. Pace; Shoemaker, I.; Sloan T.; VanDevender, A. P.; Ulmen, B.A. Mass distribution of magnetized quark-nugget dark matter and comparison with requirements and direct measurements. *Sci Rep* **2020**, *10*, 17903. <https://doi.org/10.1038/s41598-020-74984-z>
16. Oerter, R. *The Theory of Almost Everything: The Standard Model, the Unsung Triumph of Modern Physics;* Penguin Group: New York, NY, USA, 2006; 203-218.
17. VanDevender, J.P.; VanDevender, A.P.; Wilson, P.; Hammel, B.F.; McGinley, N. Limits on Magnetized Quark-Nugget Dark Matter from Episodic Natural Events. *Universe* **2021**, *7*, 35. <https://doi.org/10.3390/universe7020035>
18. Xu, R. X. Three flavors of a triangle. *Sci. China Phys. Mech. Astron.* **63**, 119531 (2020). <https://doi.org/10.1007/s11433-020-1551-0>
19. Tatsumi, T. Ferromagnetism of quark liquid. *Phys. Lett. B* **2000**, *489*, 280-286. [https://doi.org/10.1016/S0370-2693\(00\)00927-8](https://doi.org/10.1016/S0370-2693(00)00927-8)
20. Olausen, S. A.; Kaspi, V. M. The McGill magnetar catalog. *Astrophys. J. Sup.* **2014**, *212*, 1, 6. <https://doi.org/10.1088/0067-0049/212/1/6>
21. Taylor, J. H.; Manchester, R. N.; Lyne, A. G. Catalog of 558 pulsars. *Astrophys. J. Sup.* **1993**, *88*, 529-568. <https://doi.org/10.1086/191832>
22. Scherrer, R. J.; Turner, M. S. On the relic, cosmic abundance of stable, weakly interacting massive particles. *Phys. Rev. D* **33**, 1585-1589 (1986). <https://doi.org/10.1103/PhysRevD.33.1585> and *Phys.Rev.D* *34* (1986) 3263 (erratum) <https://doi.org/10.1103/PhysRevD.34.3263>
23. VanDevender, J. Pace; VanDevender, Aaron P.; Sloan, T.; Swaim, Criss; Wilson, Peter; Schmitt, Robert. G.; Zakirov, Rinat; Blum, Josh; Cross, James L.; McGinley, Niall; Detection of magnetized quark nuggets, a candidate for dark matter. *Sci. Rep.* **2017**, *7*, 8758. <https://doi.org/10.1038/s41598-017-09087-3>
24. Boslough, M. Airburst modeling. *Handbook of Cosmic Hazards and Planetary Defense*, Springer International Publishing: Switzerland, 2014. https://doi.org/10.1007/978-3-319-02847-7_56-1
25. VanDevender, J. Pace; Buchenauer, C. Jerald; Cai, Chunpei; VanDevender, Aaron P.; and Ulmen, Benjamin A.. Radio frequency emissions from dark-matter-candidate magnetized quark nuggets interacting with matter. *Sci Rep* **2020**, *10*, 13756. <https://doi.org/10.1038/s41598-020-70718-3>
26. McGlaun, J. M.; Thompson, S. L.; Elrick, M. G. CTH: A three-dimensional shock wave physics code. *Int. J. Impact Eng.* **1990**, *10*, 1-4 351-360. [https://doi.org/10.1016/0734-743X\(90\)90071-3](https://doi.org/10.1016/0734-743X(90)90071-3)
27. Crocket, S. SESAME Database: Equation-of-State tabular data for the thermodynamic properties of materials. **1999**. <https://www.lanl.gov/org/ddste/aldsc/theoretical/physics-chemistry-materials/sesame-database.php> (Date of access: 02/13/2021).
28. Duvall, W. I.; Atchison, T. C. Rock breakage by explosives. *Report of Investigations 5356*, United States Department of the Interior: USA, 1957; 1-52.
29. Starfield, A. M.; Pugliese, J. M. compression waves generated in rock by cylindrical explosive charges: a comparison between a computer model and field measurements. *Int. J. Rock. Mech. Min. Sci.* **1968**, *5*, 65-77. [https://doi.org/10.1016/0148-9062\(68\)90023-5](https://doi.org/10.1016/0148-9062(68)90023-5)

30. Boulanger, R. W.; Idriss, I. M. Liquefaction susceptibility criteria for silts and clays. *J. Geotech. & Geoenviron. Eng.* **2006**, 132, 11, 1413-1426. [https://doi.org/10.1061/\(ASCE\)1090-0241\(2006\)132:11\(1413\)](https://doi.org/10.1061/(ASCE)1090-0241(2006)132:11(1413))
31. Owen, G.; Moretti, M. Identifying triggers for liquefaction-induced soft-sediment deformation in sands. *Sedimentary Geology* **2011**, 235, 141-147. <https://doi.org/10.1016/j.sedgeo.2010.12.010>
33. Gao, Dengliang. Latest developments in seismic texture analysis for subsurface structure, facies, and reservoir characterization: A review. *Geophysics* **2011**, 76, W1-W13. <https://doi.org/10.1190/1.3553479>